Wireless Permanent Magnet Temperature & Field Distribution Measurement System for IPMSMs

Daniel Fernandez[1], David Reigosa[1], Tsutomu Tanimoto[2], Takashi Kato[2], Fernando Briz[1]
[1]University of Oviedo. Department of Electrical, Computer & System Engineering.
[2] Nissan Motor Co., Ltd, Nissan Research Center, EV System Laboratory.
diazdavid@uniovi.es, fernandezalodaniel@uniovi.es, tanimoto-t@mail.nissan.co.jp, katou-t@mail.nissan.co.jp, fernando@isa.uniovi.es

Abstract: Permanent magnet (PM) temperature measurement/estimation in permanent magnet synchronous machines (PMSMs) is of great importance for torque control and to prevent PM demagnetization. PM temperature estimation methods can be divided into thermal models, BEMF and pulse/high-frequency signal injection based methods. All of them provide a lumped PM temperature estimation. However, the temperature distribution along the magnet is not uniform, also asymmetries among poles can exist. Analyzing the impact of the temperature variations on the magnet field distribution requires simultaneous measurement of the PM temperature and field distributions. However, this is not easy due to the large amount of temperature and field sensors required, which places significant challenges regarding the sensors integration as well as the signal acquisition and transmission. Most of temperature measurement systems using contact type sensors that have been reported use a reduced amount of sensors and relatively low sampling rates. Furthermore, they do not include field sensors. This significantly limits the analysis that can be realized.

This paper presents a wireless PM temperature and field measurement system for PMSMs. The developed system provides PM temperature and field distribution maps for all the poles with high spatial resolution and bandwidth. Uses of the developed system include analysis of the surface and internal PM temperature distribution, PM field distribution, assessment of local demagnetization risks due to hot spots in PMs, as well as development and assessment of new temperature and field distribution estimation methods for PMSMs. [1]

Index Terms — Interior permanent magnet synchronous machines, PM temperature estimation, PM temperature and field measurement.

I. Introduction

Design and control of permanent magnet synchronous machines (PMSM's) have been the focus of significant research efforts during the last three decades [1-8] due to their high dynamic performance, power density and efficiency. PMSMs torque-speed characteristics strongly depends on the PM temperature. PM remanent flux, B_r, typically decreases as the temperature increases, therefore reducing the torque producing capability of the machine. This has raised the interest in the development of PM temperature measurement/estimation methods [10-26].

NdFeB magnets are the most common choice in PMSMs nowadays, though Ferrite, SmCo and Alnico magnets can also be found [9, 15-21]. Table I [9] shows typical values of the PM thermal remanent flux coefficient, which is defined as the PM remanent flux rate of variation with temperature, α_B [19-21], PM remanent flux, B_r, and the operating temperature range for commonly used PM materials [9]. The coefficient α_B is observed to vary significantly for the different materials; SmCo and Alnico magnets present low α_B values, meaning that the variation of their remanent flux (and therefore torque) with temperature is relatively small. Consequently, precise estimation of the magnet temperature is not a major concern in machines equipped with this type of magnets. On the contrary, Ferrite and NdFeB magnets present high α_B values, the variation of their remanent flux with temperature being therefore relatively large. Thus, realizing a precise control of the torque produced by machines equipping this type of magnets can require measurement/estimation of the magnet temperature. NdFeB magnets are often alloyed with dysprosium (Dy) to preserve their magnetic properties at high temperature. However, this penalizes cost, what has raised the interest in development of Dy-free magnets [5].

Table I

PM material	α_B (%/ºC)	B_r (T)	Operating temperature range (*)
Alnico 5-7	-0.02	1.35	4K to 520 ºC
Alnico 8	-0.01	0.85	4K to 520 ºC
Ferrite 8	-0.2	0.39	-40ºC to 150 ºC
Ferrite 9	-0.18	0.45	-40ºC to 150 ºC
SmCo 1:5	-0.045	0.9	4K to 520 ºC
SmCo 2:17	-0.035	1.1	4K to 520 ºC
NdFeB 33EH	-0.11	1.15	150K to 200 ºC
NdFeB 48M	-0.12	1.39	150K to 100 ºC

(*) ºC and K are used as this is the format used by the manufacturer [9].

PMs, SmCo, Alnico, ferrite or NdFeB, can also suffer irreversible demagnetization, which might occur under certain PM temperature and loading (i.e. i_{dq} current) conditions. Demagnetization of PMs in PMSMs has been extensively studied [6, 27, 28], it can occur locally (partial demagnetization) or globally (uniform demagnetization) [6].

[1] This work was supported by Nissan motor Co. Ltd..

The maximum temperature that a PM can reach without irreversible demagnetization defines its maximum working temperature. As it can be observed from Table I [8], SmCo and Alnico magnets operating temperature range is wide compared to NdFeB and Ferrite magnets. In all the cases, demagnetization due to temperature occurs at well defined limit, meaning that a high accuracy estimating the temperature is needed to prevent demagnetization if the machine is expected to operate near its limit. It is concluded from the previous discussion that measuring/estimating the magnet temperature distribution is highly desirable for torque control/monitoring purposes and to prevent demagnetization.

Eq. (1) shows the relationship between the PM temperature and field, where $B_{r(T)}$ is the magnet flux at a temperature T, $B_{r(T_0)}$ is the remanent PM flux at the room temperature and T_0 is the room temperature. It is observed from (1) that the PM field typically decreases as temperature increases [9, 19-21], see Table I.

$$B_{r(T)} = B_{r(T_0)}\left(1+\alpha_B\left(T-T_0\right)\right) \quad (1)$$

Both PM temperature and field can be measured or estimated. PM temperature [10-14,19-23, 25] and field estimation methods [15-18, 32, 33] developed up to date assume a uniform temperature and field distribution along the magnet. Therefore, they do not consider the effects of a non-uniform PM temperature and/or field distributions, as asymmetries in the temperature or in the field distribution among magnets for each pole. Therefore they are not suitable to study these effects, and their impact on e.g. partial (local) demagnetization due to temperature. On the other hand, PM temperature measurement systems reported in the literature typically include IR camera, [19], a single IR sensor [20] or an array of contact type sensors (i.e. thermocouples) [21-26]. In all cases, the information that they provide is insufficient to build a temperature map of the magnets. Further limitations of these systems is that they measure the temperature at the PM surface PM, i.e. do not provide information on the PM internal temperature distribution, and in most of the cases [18-20] the temperature of only one magnet is measured, study of temperature asymmetries between PMs not being therefore possible.

PM field measurement is difficult compared to temperature measurement. PM field can be measured by inserting a magnetometer in the airgap of the machine. However, this requires to remove or drill the end frame of the machine to insert the field sensor. Also, the magnetometer has to be placed on the magnet surface, which is only feasible with SPMSMs and if the machine is not rotating. To the best of authors' knowledge, no PM field measurement systems for IPMSM have been developed up to date. Alternatively, PM remanent flux could be indirectly estimated using (1), assumed that the magnet temperature is known. However, validation of this approach would require the use of a field sensor, capable of providing a field map of the magnet.

A wireless PM temperature and field distribution measurement system for IPMSMs is presented in this paper. The final use of this system is the development of advanced PM temperature and field estimation methods. The proposed system does not interfere with the normal operation of the machine. It provides PM temperature and field maps in real time for all the magnets with high spatial resolution and sampling rates. Potential uses of the proposed system include measurement of the PM temperature and field distributions, evaluation of the asymmetries among magnets in the temperature and field distribution (e.g. due to lamination grain orientation) and evaluation of local demagnetization risks due to hot spots in PMs. Furthermore, by combining the PM surface temperature and field distributions measurements, it would be possible to estimate the internal PM temperature distribution. The proposed system can also potentially be used for the development and assessment of new temperature and field distribution estimation methods for PMSMs.

The paper is organized as follows: a review of PM temperature and field estimation methods and PM temperature measurement systems is presented in section II and III respectively. The proposed PM temperature and field measurement system is presented in section IV. Finally, experimental results showing the viability of the proposed system is presented in section V.

II. Review of PM temperature & field estimation methods

Several methods have been proposed for PM temperature and field estimation [10-23, 32, 33]. All of them assume a uniform temperature and field distribution along the magnet, and do not provide therefore any information on the spatial distribution. The existing methods are briefly reviewed following:

a) PM Temperature estimation methods

PM temperature estimation methods can be divided into thermal models [10-14], BEMF based methods [15-18] and methods based on the injection of some form of test signal [19-23].

- Thermal models consist of thermal nodes which represent uniform temperature regions. The thermal nodes are connected by thermal resistances, which represent the heat transfer. Power sources represent the machine power losses (i.e. magnet, copper and core losses), while heat capacitors represent the heat storage capability for the different parts of the machine. Building a thermal model requires therefore knowledge of the stator and rotor geometry, materials and cooling system. Consequently, thermal models need to be calibrated for each specific machine.
  Thermal models are normally based on a 2D machine model, a constant temperature in the axial direction is therefore assumed. In addition they do not consider thermal asymmetries between magnets (e.g. due to lamination grain orientation).

- BEMF methods and methods based on the injection of a test signal estimate the magnet temperature form the measured stator electrical variables (voltage and currents) [15-23]. BEMF based methods estimate the magnet temperature from the PM flux linkage [15-18] while methods based on the injection of a test signal estimate the magnet temperature from the machine high frequency resistance or inductance [19-23], both being function of the PM temperature. Both types of methods are relatively easy to implement, being therefore very popular.

b) PM Field estimation methods

These methods estimate the rotor PM flux linkage from the measured stator voltages and currents [15-18, 32-33]. They provide an average value of PM flux linkage. Consequently, they do not provide any information on the PM field distribution within the magnet, or asymmetries among magnets.

III. Review of temperature measurement systems

PM temperature measurement in PMSM is not trivial. Existing solutions can be separated into non-contact and contact type sensors; both types are briefly discussed following.

a) Non-contact type sensors

Non-contact type sensors (i.e. IR) [19, 20] require the magnet surface to be visible. This is viable in many SPMSM designs, but is not feasible in most IPMSM designs. Further concerns for this type of sensors include price, accuracy, mounting issues and reduced robustness. The use of an infrared camera was presented in [19]. The measurement system was used in two SPMSMs, in which the magnets surfaces were visible. The system required drilling the machine end frame to have access to the magnet, compromising therefore the machine robustness. The IR camera measures the side face of the magnet, PM temperature distribution measurement in the axial direction not being therefore feasible. The use of an infrared thermometer was presented in [20]. Though it is significantly cheaper than the IR camera [19], it suffers from the same limitations.

b) Contact type sensors

To overcome some of the limitations of non-contact type sensors, the use of contact type sensors have been proposed [21, 23-26]. Contact type sensors (e.g. PTC thermistors…) require the use of slip rings and brushes, or alternatively of a wireless transmission system. In all cases the prototypes that have been developed up to date provide either a single measurement or the PM temperature distribution in one dimension. A measurement system of this type is described in [24]. Targeted to induction machines, the rotor was equipped with 6 thermocouples. The method in [24] was extended to IPMSMs in [23, 25, 26]. It uses 4 thermocouples to measure the temperature at different locations of the magnet, the remaining two being used to measure the rotor yoke temperature. While this system provides information on the temperature distribution along the magnet, the spatial resolution is small, and do not allow to measure asymmetries among poles. In the system reported in [21] for IPMSMs, the rotor was equipped with 13 thermocouples located along one PM. The thermocouples signals were connected throughout a hollow shaft, and to a measurement and wireless transmission sub-system. Therefore, this system measures the PM temperature in the axial direction. However, it does not provide any information on the temperature distribution in the tangential direction and on asymmetries among PMs.

It is concluded that the performances of the prototypes reported in [21, 23-26] have a limited spatial resolution, and do not allow to measure asymmetries among poles

IV. High resolution PM temperature and field measurement system

This section describes the design of a high resolution temperature and field measurement system. It consist of an array of temperature sensors, which are attached to the PMs. Identical arrays are mounted on each magnet, detection of asymmetries among poles e.g. due to lamination grain orientation, being feasible. In addition to the temperature sensors, an array of field sensors is also inserted, which could be potentially used to study the relationship between the temperature and the field strength.

Fig. 1 schematically shows the developed temperature and field measurement system. Green and red dots in the permanent magnets (PM-1 to 6) represent the field and temperature sensors respectively. Each sensors array consists of 15 temperature and field sensors in a 3x5 arrangement.

TMP100 digital temperature sensors with I^2C interface (serial 2-wire) have been used [29]. They provide a resolution of 0.0625ºC, with a maximum operating temperature of 125ºC. The I^2C bus can operate at frequencies above 3.4Mbits/s, i.e. the 15 temperature sensors can be read at a maximum frequency of ≈14kHz, which is fast enough, considering the machine thermal time constant [19-21]. Each I^2C bus is connected to the corresponding I^2C port of a *PIC24FJ64GA004* microcontroller (Slave *µController-1 to 12* in Fig. 1) [30]. I^2C allows connection of up to eight sensors to each I^2C, significantly reducing the number of wires throughout the hollow shaft compared to other implementations [21].

Hall-effect mono-crystal gallium arsenide (GaAs) sensors have been used to measure the field [31]. Their measuring range is 0-3T, which is adequate to measure the PM field in PMSMs, typically in a range of 0-1.8T. Their maximum operating temperature is 125ºC, which is the same as for the temperature sensors. The output of the field sensors is an analog voltage, which is adapted and filtered (see *"filtering & conditioning"* in Fig. 1), and further connected to the A/D converter of the slave *µController-1 to 12* in Fig. 1. Two

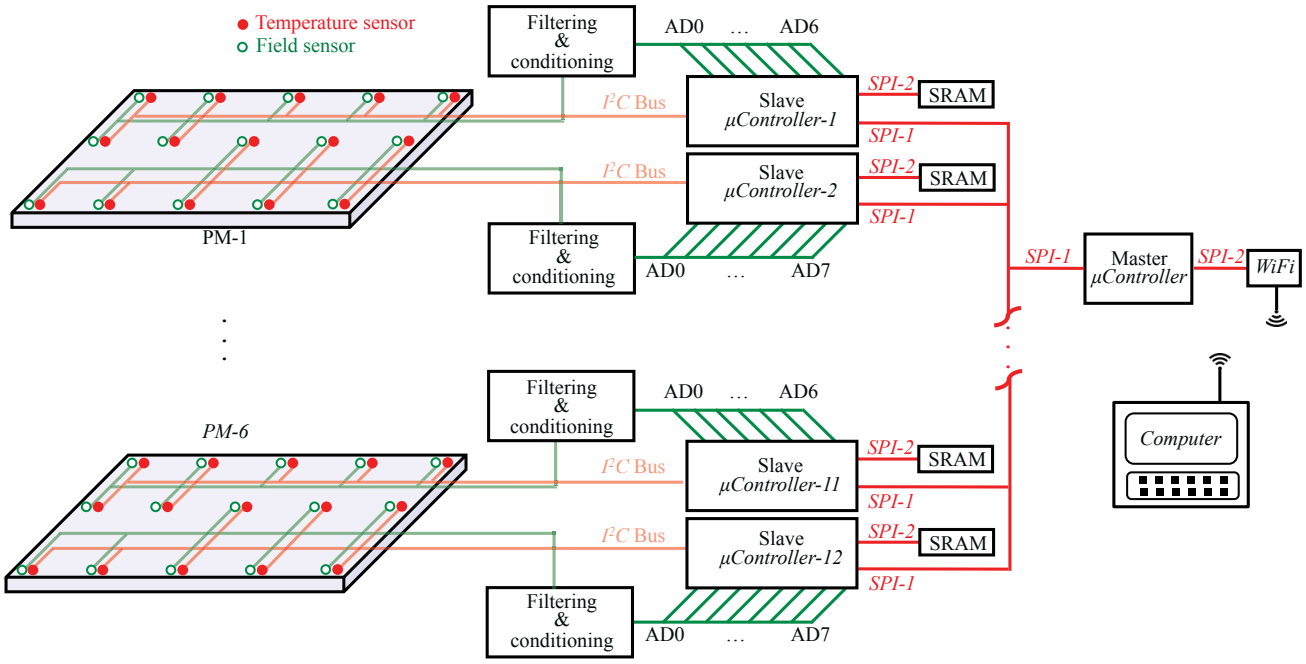

Fig. 1.- Schematic representation of the temperature and field measurement system.

microcontrollers, each with 8 A/D channels, are used (see Fig. 1).

Slave *µControllers*, 1 to 12, are connected via *SPI* to a master *µController* (see Fig. 1). The master *µController* periodically collects temperature and field measurements from all slave *µControllers*, which are transmitted to a central computer using a *WiFi* link. The baud rate limit due to the *WiFi* link is 230kbits/s, i.e. the 15 temperature sensors and the 15 field sensors can be read at a maximum frequency of 550Hz. While this is fast enough for PM temperature transmission, it can be insufficient for field measurement, as this can change significantly faster. To fully exploit the bandwidth of the field sensors, a *SPI SRAM* memory (1024 kbits) has been connected to the SPI-1 port of each slave *µController*. The *SPI SRAM* memory baud rate is 16Mbits/s, i.e. the 15 field sensors can be read at a maximum frequency of ≈172kHz, which is fast enough to store the field variations with an adequate bandwidth. The data stored in the *SRAM* memory is later accessed and transmitted to the computer via the *WiFi* Link.

Fig. 2a shows the field and temperature 3x5 sensors array distribution. Fig. 2b shows the array of sensors mounted on a flexible PCB. Fig. 2c shows the six flexible PCBs during rotor assembling, one per magnet. All the PCBs are connected to the *connection PCB* shown in Fig. 2d, which is mounted on the shaft. Fig. 2e shows the flexible PCBs and the *connection PCB* after assembling the rotor. All the I^2C buses are connected to the slave *µControllers* throughout a hollow shaft using the flexible PCBs shown in Fig. 2e, (see Fig. 2f). The filtering and conditioning stages, slave *µControllers,* master *µController*, *SRAM* memories and *WiFi* module are assembled into an aluminum box that it is coupled to the machine shaft (Fig. 2g and 2h). Table II summarizes the main characteristics.

Table II: System characteristics

	Temperature	Field
Sensor temp. limit	125ºC	125ºC
Resolution	0.0625ºC	0.001T
Measuring range	-55ºC to 125ºC	0-3T
Bandwidth	14kHz	50kHz

V. Experimental results

The proposed system has been tested on an IPMSM (see Fig. 2). The machine parameters are shown in Table I. Experimental results of both temperature and field measurement systems are shown in this section.

a) Temperature measurement

Fig. 3 shows the PM temperature measured by the sensors array, when I_q current changes from 0 to 1pu in steps of 0.2 pu. No *d*-axis current was injected (I_d =0), MTPA not being implemented therefore. Consequently, the observed temperature variations are due exclusively to the *q*-axis current. Fig. 4 shows the same experimental results as in Fig. 3 but for the case of I_d current changing from 0 to -1pu in steps of 0.2pu, with no *q*-axis current being injected. The results shown in Fig. 3 and Fig, 4 were taken 30 min. after the corresponding change in the

Table II: Machine parameters				
P_R [kW]	V_R [V]	I_R [A]	f_R[rpm]	P
7.5	300	14.5	1800	6

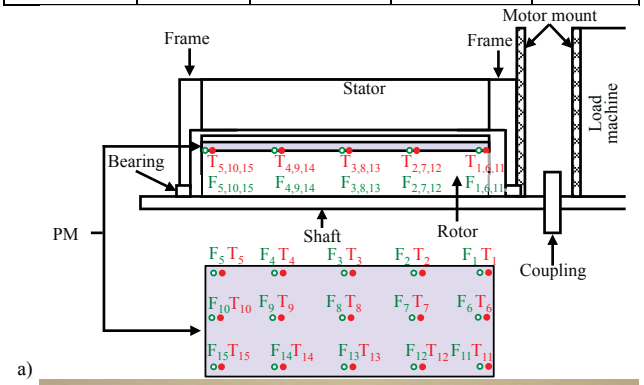

a)

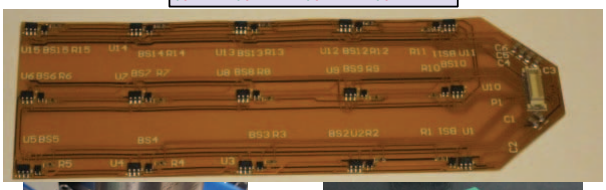

b)

c)

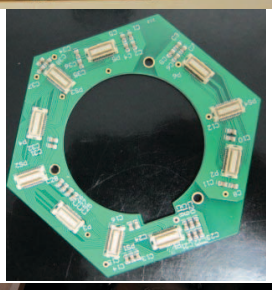

d)

e)

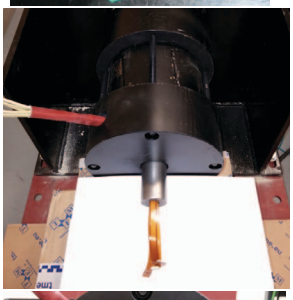

f)

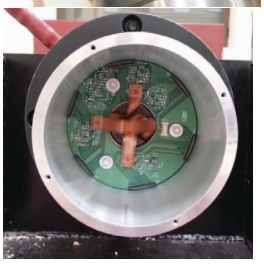

g)

h)

Fig. 2.- a) Temperature and field sensors array; b) sensors array mounted on a flexible PCB; c) rotor assembling; d) connection PCB; e) assembled rotor and connection PCBs; f) hollow shaft and connection PCBs; g) assembling of the connection PCB; h), aluminum box containing master *µController* PCB, Slave *µControllers* PCBs, filtering and conditioning PCBs and *WiFi* module.

current. It can therefore be assumed that the machine had

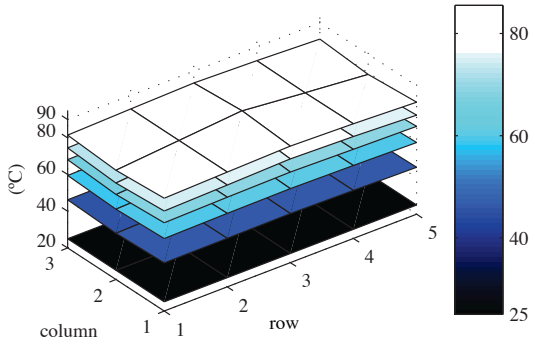

Fig. 3.- Experimentally measured magnet temperatures for I_q current of: 0, 0.2, 0.4, 0.6 ,0.8 and 1. I_d=0 pu, ω_r =2*π*50 rad/s.

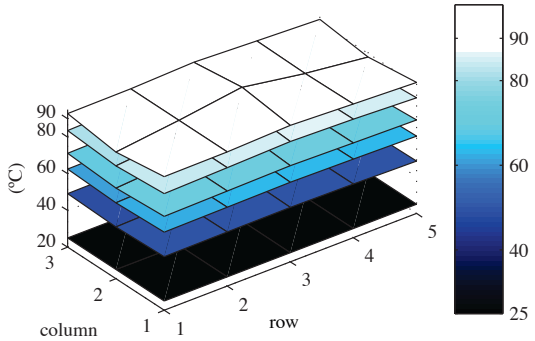

Fig. 4.- Experimentally measured magnet temperatures for I_d current of: 0, 0.2, 0.4, 0.6 ,0.8 and 1. I_q=0 pu, ω_r =2*π*50 rad/s.

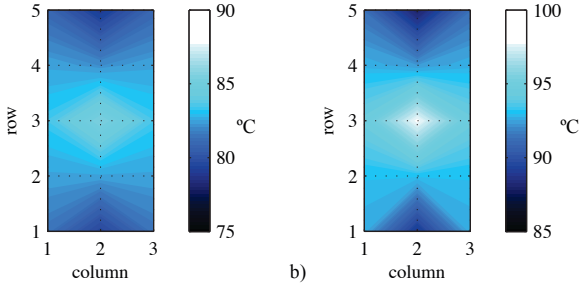

Fig. 5.- Detail of the experimentally measured magnet temperature, for I_q=1pu, a), and I_d=-1pu, b). ω_r =2*π*50 rad/s.

reached its thermal equilibrium.

It is observed that both *d* and *q*-axis currents increase the magnet temperature, *d*-axis current producing larger temperature increases. This is due to the combined effect of the increased airgap flux harmonic content due to the I_d current injection [34] and magnetorresistive effect [35]. When I_d current is injected, e.g. for flux-weakening, the reflected stator magnet high frequency resistance increases [35], increasing therefore the induced magnet losses and consequently the magnet temperature.

Fig. 5a and 5b show the experimentally measured magnet temperature for two particular cases: I_q=1pu and I_d=−1pu respectively. It is observed that both *d* and *q*-axis currents induce

non-uniform magnet temperature distributions. The magnet temperature is higher at the central part of the magnet, the risk of demagnetization being therefore higher in this region. It is also observed that the temperature distribution is non-symmetric respect to the mid row (row 3), i.e. temperatures measured by sensors in row 1 are higher than sensors in row 5. Sensors in row 1 are the closest to the mechanical coupling with the load machine, (see Fig. 2a), the heat transfer between the IPMSM and the load IM through the mechanical coupling being a potential explanation for this behavior. It is also observed that the magnet temperature is slightly higher at the corners, (i.e. T_1, T_5, T_{11} and T_{15}) compared to the edges (T_6 and T_{10}). This could be due to the fact that magnet corners are closer to the airgap, being therefore more affected by airgap-flux harmonics. This issue is further discussed in the next subsection using the field measurement.

b) Field measurement

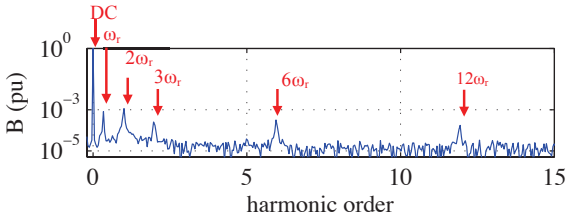

Fig. 6.- Experimentally measured magnet field. ω_r=2*π*50 rad/s I_d=-1pu, I_q=0pu. Though not shown in the figure, no relevant harmonics exist higher than 12th.

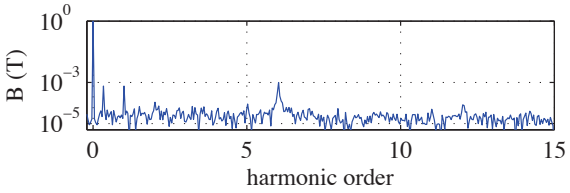

Fig. 7.- Experimentally measured magnet field. ω_r=2*π*50 rad/s, I_d=0pu, I_q=1pu.

The field sensors are sampled at 50kHz, the measurements being stored in the *SPI SRAM* memory (see Fig. 1), being later transmitted to the computer via *WiFi* link.

Fig. 6 and 7 shows the FFT of the field measurement provided by the central field sensor (*F8* in Fig. 2a), and for two different values of the current: I_d=-1pu and I_q=0pu; I_d=0pu and I_q=1pu. In both cases the machine was rotating at ω_r=2*π*50 rad/s. Six major components can be observed: DC, $1\omega_r$, $2\omega_r$, $3\omega_r$, $6\omega_r$ and $12\omega_r$. The DC component represents the mean PM magnetic field, the rest of components resulting from the combined effect of the stator slotting and rotor magnets (poles). It is noted that the harmonic content of the measured field remains invariant with respect to the speed.

It is observed from Fig. 6 and 7 that the harmonic content in both cases, i.e. I_d or I_q current injection, is very similar. However, the magnitude of the harmonic components are larger for the case of I_d current injection. This will result in increased stator, rotor and magnet losses, and consequently higher magnet temperature. This is consistent with the measured magnet temperatures shown in Fig. 3 and 4.

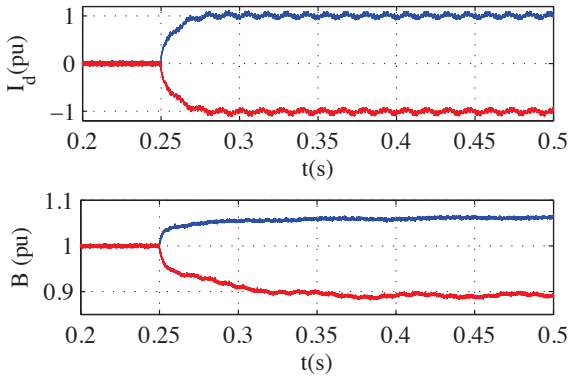

Fig. 8.- Experimentally measured d-axis current a) measured transient response of the magnet field b). ω_r =2*π*50 rad/s.

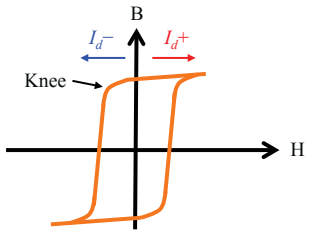

Fig. 9.- Generic B-H curve of a PM.

Fig. 8 shows the experimentally measured transient response of the magnetic field sensor *F8* (see Fig. 2a) after positive and negative step-like changes of the *d*-axis current. It is observed that the transient response following the positive I_d current step is faster than the transient following the negative step, meaning that, for the same dynamic behavior of the *d*-axis current, intensification of the magnetic field occurs faster than weakening. There is not clear explanation for this behavior, this issue being currently subject of study. It is also observed that incremental variation of the PM field following the positive step of the *d*-axis current is smaller than the incremental variation for the negative step case. This behavior can be easily explained by the B-H curve shown in Fig. 9. When positive I_d current is injected, the permanent magnet, and also the stator and rotor cores, become more saturated, meaning that lower magnet field variations would be obtained for a fixed I_d current step like change. On the contrary, negative I_d current leads to a less saturated core, closer therefore to the saturation knee. Larger magnet field variations are expected in this case for the same I_d current change.

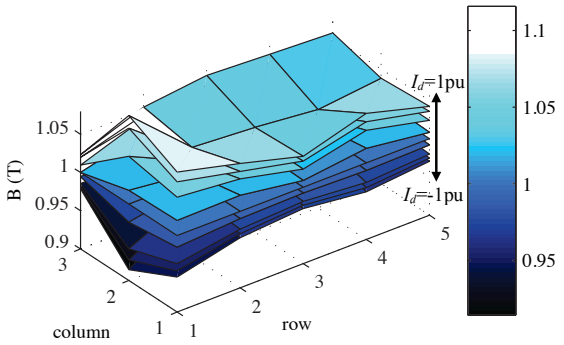

Fig. 10.- Experimentally measured magnet field for I_d = -1, -0.75, -0.5, -0.25, 0, 0.25, 0.5 ,0.75 and 1pu respectively. I_q=0 pu, ω_r =2*π*50 rad/s.

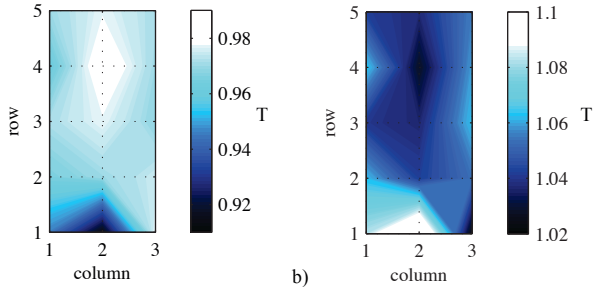

Fig. 11.- Experimentally measured magnet field, for a) I_d=-1pu and b) I_d=1pu. ω_r =2*π*50 rad/s.

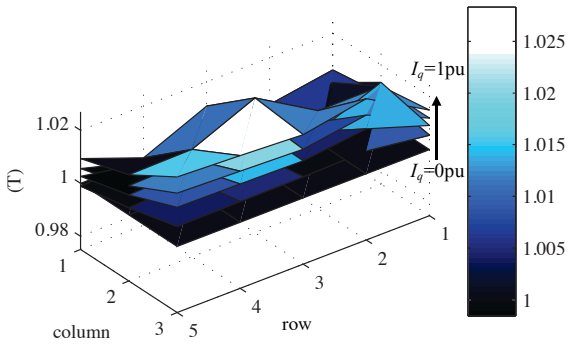

Fig. 12.- Experimentally measured magnet field for I_q = 0, 0.25, 0.5 ,0.75 and 1 pu respectively. I_d=0 pu, ω_r =2*π*50 rad/s.

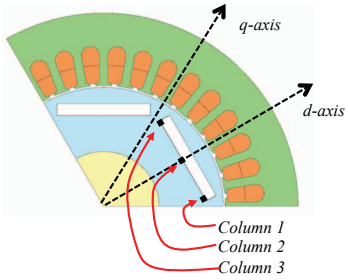

Fig. 13.- Schematic representation of *dq*-axes respect sensor array.

Fig. 10 shows the mean PM field (DC component in Fig. 6 and 7), measured by the field sensors array, when I_d changes from -1, i.e. flux weakening current, to 1pu, i.e. flux intensifying current, in steps of 0.25 pu, no *q*-axis current was injected (I_q =0). Fig. 11 shows the PM field distribution for I_d=1pu and I_d=−1pu.

It is observed from Fig. 10 and 11 that the PM field distribution is not uniform when *d*-axis current is injected; field sensors in row 1 being more affected by *d*-axis current injection. This behavior was not expected and is being studied at the moment. In addition, field sensors in the central region of the magnet, i.e. *F7*, *F8* and *F9* in Fig. 2, are less affected by the *d*-axis current than the rest of field sensors. This result suggests that it is easier to weaken or intensify the magnet edges than the central region of the magnet. This could be explained by the eddy currents induced in the magnets due to the *d*-axis current injection.

Fig. 12 shows the same experimental results as in Fig. 10 but for the case of I_q changing from 0 to 1pu, with no *d*-axis current being injected (I_d =0). Field variations are therefore due exclusively to the *q*-axis current in this case. As expected, *q*-axis current induces PM field variation due to the cross-coupling that typically exists between *d* and *q*-axes.

As for the *d*-axis current injection case, *q*-axis current injection induces a non-uniform PM field distribution, which is not symmetric with respect column 2 (see Fig. 13). Field measured by sensors in column 3, (i.e. closer column to the machine *q*-axis), is larger than that of sensors in column 1 (closer column to the machine negative *q*-axis). Experimental injecting negative *q*-axis current show the same trends. This non-symmetrical field distribution due to *q*-axis current injection was not expected and is also a subject of study.

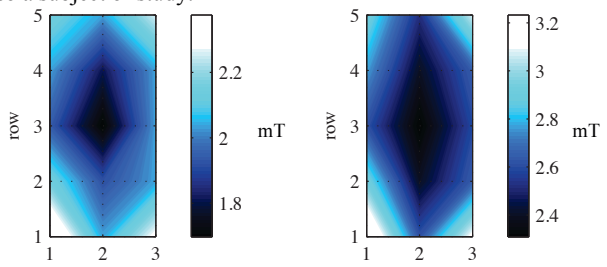

Fig. 14.- Experimentally measured harmonic component of the magnet field at a) $6\omega_r$ and b) 12ω . I_d=-1pu, ω_r =2*π*50 rad/s.

Finally, Fig. 14 shows the measured $6\omega_r$ and $12\omega_r$ harmonic components (see Fig. 6 and 7). It is observed that they have larger magnitude at the magnet corners. This was an expected result, as the magnet corners are closer to the airgap, being therefore more sensitive to airgap flux harmonics. These preliminary results suggest that the magnet corner losses will be higher than the central magnet losses, which can contribute to an increase of the magnet temperature in the magnet corners vs. the edges. This is consistent with the magnet temperature measurements shown in Fig. 3-5. These preliminary results demonstrate the existence of a correlation between the PM field harmonics and the PM

temperature. This issue is currently the focus of intensive investigation.

VI. Conclusions

Design and construction of a PM temperature and field distribution measurement system for IPMSMs is presented in this paper. The spatial resolution and sampling rates enable precise and highly dynamic measurements, overcoming the limitations of other systems reported in the literature. Simultaneous measurement of the temperature and magnetic field allows a precise assessment of the risks of global or partial demagnetization, the study of the correlation between the magnet temperature and the magnetic field, as well as the assessment and validation of temperature and field estimation methods.

VII. References

[1] N. Bianchi and T. M. Jahns "Design, Analysis, and Control of Interior PM Synchronous Machines," Tutorial Course Notes, IEEE-IAS'04, Oct. 2004.

[2] K. Akatsu and S. Wakui, "Torque and Power Density Comparison Between Fractional-Slot Concentrated Winding SPMSMs", Intl. Conf. on Elect. Machines & Systems, CD-ROM, Nov. 2006, Nagasaki.

[3] K. Akatsu, K. Narita, Y. Sakashita and T. Yamada, "Characteristics Comparison Between SPMSM and IPMSM Based on both Analytical and Experimental Results", Intl. Conf. on Elect. Machines & Systems, CD-ROM, Oct. 2008, Wuhan, China.

[4] J. F. Gieras and M. Wing, "Permanent Magnet Motor Technology: Design and Application". Second edition 2002.

[5] J. D. McFarland, T. M. Jahns, A. M. El-Refaie, P. B. Reddy, "Effect of Magnet Properties on Power Density and Flux-Weakening Performance of High-Speed Interior Permanent Magnet Synchronous Machines ", IEEE-ECCE, pp. 4218-4225, Sept. 2014.

[6] S. Ruoho, J. Kolehmainen, J. Ikaheimo and A. Arkkio,"Interdependence of Demagnetization, Loading, and Temperature Rise in a Permanent-Magnet Synchronous Motor," IEEE Trans. Magn., vol. 46, no. 3, pp. 949–953, Mar. 2010.

[7] M. Kamiya, Y. Kawase, Y. Kosada and N. Matsui, "Temperature Distribution Analysis of Permanent Magnet in Interior Permanent Magnet Synchronous Motor Considering PWM Carrier Harmonics," IEEE-ICEMS, pp. 2023–2027, Oct. 2007.

[8] P. Milanfar and J. H.Lang, "Monitoring the Thermal Condition of Permanent-Magnet Synchronous Motors," IEEE Trans. on Aerospace and Electronic Systems, 32(4): 1421-1429, Oct. 1996.

[9] www.arnoldmagnetics.com

[10] A. M. EL-Refai, N. C. Harris, T. M. Jahns,K. M. Rahman, "Thermal Analysis of Multibarrier Interior PM Synchronous Machine Using Lumped Parameter Model". IEEE Trans. on Energy Conv., 14(2):303–309, June 2004.

[11] C. Kral, A. Haumer and S. B. Lee, "A Practical Thermal Model for the Estimation of Permanent Magnet and Stator Winding Temperatures". IEEE Trans. on Pow. Elect., 29(1):455–464, Jan. 2014.

[12] B.-H. Lee , K.-S- Kim , J.-W. Jung , J.-P. Hong and Y.-K. Kim, "Temperature Estimation of IPMSM Using Thermal Equivalent Circuit ". IEEE Trans. on Mag., 48(11):2949–2952, Nov. 2012.

[13] A. J. Grobler, S. R. Holm and G. van Schoor, "Thermal Modeling of a High Speed Permanent Magnet Synchronous Machine". IEEE-IEMD, pp.319–324, May. 2013.

[14] T. Huber, W. Peters and J. Böcker, "A Low-Order Thermal Model for Monitoring Critical Temperatures in Permanent Magnet Synchronous Motors ". IET-PEMD, pp. 1–6, April 2014.

[15] K. Liu and Z. Q. Zhu "Online Estimation of the Rotor Flux Linkage and Voltage-Source Inverter Nonlinearity in Permanent Magnet Synchronous Machine Drives," IEEE Trans. on Pow. Elect., 29(1): 418-427, Jan. 2014.

[16] K. Liu and Z.Q. Zhu "Mechanical Parameter Estimation of Permanent Magnet Synchronous Machines with Aiding from Estimation of Rotor PM Flux Linkage", IEEE-ECCE, pp.4850-4857, Sept. 2014.

[17] S. Underwood, and I. Husain, "On-line Parameter Estimation and Adaptive Control of Permanent Magnet Synchronous Machines," IEEE Trans. Ind. Electron., vol. 57, no. 7, pp. 2435-2443, Jun. 2010.

[18] S. Ichikawa, M. Tomita, S. Doki, and S. Okuma, "Sensorless Control of Permanent-Magnet Synchronous Motors Using Online Parameter Identification Based on System Identification Theory," IEEE Trans. Ind. Electron., vol. 53, no. 2, pp. 363-372, Apr. 2006.

[19] D. Reigosa, F. Briz, P. García, J. M. Guerrero and M. W. Degner, "Magnet Temperature Estimation in Surface PM Machines Using High Frequency Signal Injection". IEEE Trans. on Ind. Appl., 46(4): 1468–1475, July-Aug. 2010.

[20] D. Reigosa, F. Briz, M. W. Degner, P. García and J. M. Guerrero, "Magnet Temperature Estimation in Surface PM Machines During Six-Step Operation". IEEE Trans. on Ind. Appl., 48(6): 2353–2361, Nov.-Dec. 2012.

[21] D. Reigosa, D. Fernandez, H. Yoshida, T. Kato and F. Briz "Permanent magnet temperature estimation in PMSMs using pulsating high frequency current injection," IEEE-ECCE'14, pp. 1729-1736, Sept. 2014.

[22] M Ganchev, C. Kral and T. Wolbank, "Compensation of Speed Dependency in Sensorless Rotor Temperature Estimation for Permanent-Magnet Synchronous Motors," IEEE Trans. on Ind. Appl., 49(6): 2487-2495, Nov.-Dec. 2013.

[23] M Ganchev, C. Kral, H. Oberguggenberger and T. Wolbank, "Sensorless Rotor Temperature Estimation of Permanent Magnet Synchronous Motor," IEEE IECON, pp. 2018-2023, Nov. 2011.

[24] M. Ganchev, B. Kubicek and H. Kappeler, "Rotor Temperature Monitoring System", ICEM, pp. 1-5, Sept. 2010.

[25] M. Ganchev, H. Umschden and H. Kappeler, "Rotor Temperature Distribution Measuring System", IEEE-IECON, pp. 2006-2011, Nov. 2011.

[26] C. Kral, A. Haumer and S. B. Lee, "Innovative Thermal Model for the Estimation of Permanent Magnet and Stator Winding Temperatures", IEEE-ECCE, pp. 2704-2711, Set. 2012.

[27] K. C. Kim, S. B. Lim, D. H. Koo and J. Lee, "The Shape Design of Permanent Magnet for Permanent Magnet Synchronous Motor Considering Partial Demagnetization", IEEE Trans. on Mag., 42(10): 3485–3487, Oct. 2006.

[28] D. Torregrossa, A. Khoobroo and B Fahimi," Prediction of Acoustic Noise and Torque Pulsation in PM Synchronous Machines With Static Eccentricity and Partial Demagnetization Using Field Reconstruction Method", IEEE Trans. on Ind. Elect., 59(2): 934–944, Feb. 2012.

[29] www.ti.com/lit/ds/sbos231g/sbos231g.pdf

[30] www.microchip.com.tw/Data_CD/Datasheet/16-Bits/39881B.pdf

[31] www.hallsensors.de/CYSJ106C.pdf

[32] X. Xiao, C. Chen and M. Zhang, "Dynamic Permanent Magnet Flux Estimation of Permanent Magnet Synchronous Machines", IEEE Trans. on Appl. Sup., 20(3): 1085–1088, June. 2010.

[33] T. J. Vyncke, R. K. Boel and J. A. A. Melkebeek, "A Comparison of Stator Flux Linkage Estimators for a Direct Torque Controlled PMSM Drive", IEEE IECON 20(3): 971–978, Nov. 2009.

[34] Qi Li, Tao Fan , Xuhui Wen, and Puqi Nin, "An Analytic Analysis Approach of Magnet Eddy-Current Losses for Interior Permanent Magnet Synchronous Machines during Flux Weakening" IEEE Trans. on Mag., early access article 2015.

[35] D. Reigosa, D. Fernandez, Z.Q. Zhu and F. Briz, "PMSM Magnetization State Estimation Based on Stator-reflected PM Resistance Using High Frequency Signal Injection", IEEE Trans. on Ind. Appl., 51, early access article Sept.-Oct. 2015.